1-1-2013

Mixed-metal (Li, Al) amidoborane: synthesis and enhanced hydrogen storage properties

Guanglin Xia
University of Wollongong, gx168@uowmail.edu.au

Yingbin Tan
Fudan University

Xiaowei Chen
Fudan University

Zaiping Guo
University of Wollongong, zguo@uow.edu.au

Hua-Kun Liu
University of Wollongong, hua@uow.edu.au

See next page for additional authors

Mixed-metal (Li, Al) amidoborane: synthesis and enhanced hydrogen storage properties

Abstract

Mixed-metal (Li, Al) amidoborane has been synthesized via mechanical ball milling of ammonia borane with lithium hexahydridoaluminate in different molar ratios. The reversible dehydrogenation properties of the thus-synthesized metallic amidoborane and its mixtures with ammonia borane in different ratios were systematically investigated in comparison with neat ammonia borane (AB). On the basis of thermogravimetric analysis and mass spectrometry results, the thus-synthesized mixed-metal amidoborane was shown to release around 10 wt% hydrogen below 200 degrees C, with an effective suppression of volatile side products. Furthermore, a synergistic effect between metallic amidoborane and ammonia borane has been identified, which leads to the release of 9 wt% hydrogen with high purity at 120 degrees C. Additionally, upon treatment with hydrazine in liquid ammonia, the regenerated products from the decomposed Li3AlH6-nAB (n = 4, 5, and 6) composites can release 3.5 wt% hydrogen with high purity, corresponding to an approximate 35%, 30%, and 26% regeneration yield for the post-milled Li3AlH6-nAB (n = 4, 5, and 6) composites, respectively.

Keywords

amidoborane, al, properties, li, storage, metal, mixed, hydrogen, enhanced, synthesis

Disciplines

Engineering | Science and Technology Studies

Publication Details

Xia, G., Tan, Y., Chen, X., Guo, Z., Liu, H. & Yu, X. (2013). Mixed-metal (Li, Al) amidoborane: synthesis and enhanced hydrogen storage properties. Journal Of Materials Chemistry A, 1 (5), 1810-1820.

Authors

Guanglin Xia, Yingbin Tan, Xiaowei Chen, Zaiping Guo, Hua-Kun Liu, and Xuebin Yu

Journal of Materials Chemistry A

RSC Publishing

PAPER

View Article Online
View Journal | View Issue

Mixed-metal (Li, Al) amidoborane: synthesis and enhanced hydrogen storage properties†

Cite this: *J. Mater. Chem. A*, 2013, **1**, 1810

Guanglin Xia,[ab] Yingbin Tan,[a] Xiaowei Chen,[a] Zaiping Guo,*[bc] Huakun Liu[b] and Xuebin Yu*[a]

Mixed-metal (Li, Al) amidoborane has been synthesized *via* mechanical ball milling of ammonia borane with lithium hexahydridoaluminate in different molar ratios. The reversible dehydrogenation properties of the thus-synthesized metallic amidoborane and its mixtures with ammonia borane in different ratios were systematically investigated in comparison with neat ammonia borane (AB). On the basis of thermogravimetric analysis and mass spectrometry results, the thus-synthesized mixed-metal amidoborane was shown to release around 10 wt% hydrogen below 200 °C, with an effective suppression of volatile side products. Furthermore, a synergistic effect between metallic amidoborane and ammonia borane has been identified, which leads to the release of 9 wt% hydrogen with high purity at 120 °C. Additionally, upon treatment with hydrazine in liquid ammonia, the regenerated products from the decomposed Li_3AlH_6–*n*AB ($n = 4$, 5, and 6) composites can release 3.5 wt% hydrogen with high purity, corresponding to an approximate 35%, 30%, and 26% regeneration yield for the post-milled Li_3AlH_6–*n*AB ($n = 4$, 5, and 6) composites, respectively.

Received 14th October 2012
Accepted 30th November 2012

DOI: 10.1039/c2ta00697a

www.rsc.org/MaterialsA

1 Introduction

In an effort to reduce global warming and the world's dependence on fossil fuels, there has been a strong push towards the so-called hydrogen economy, because hydrogen has the highest energy density of all, and more importantly, water is the only waste product when hydrogen is used in a fuel cell.[1] Both the generation and storage of hydrogen in sufficient quantities are very challenging problems that need to be overcome for hydrogen technology to be commercialized. Unfortunately, even after several decades of intensive investigation, up to now, no single hydrogen storage material fulfills all the essential application requirements, *e.g.*, volumetric and gravimetric hydrogen capacities, handling pressure and temperature, and regeneration of dehydrogenated products.

Ammonia borane (BH_3NH_3, AB hereafter), with 19.6 wt% hydrogen capacity and good stability under ambient conditions, as well as recently demonstrated regenerability,[2] has been extensively investigated as a potential hydrogen storage candidate.[3] The relatively high temperature of hydrogen release (over 100 °C), however, and the accompanying evolution of volatile by-products (*i.e.*, ammonia, borazine, and diborane), together with its severe foaming and volume expansion during thermal decomposition, significantly hinder the practical application of AB as a hydrogen storage material. To date, many efficient strategies have been adopted, such as nanoconfinement using nanoscaffolds,[4] catalysis effects,[5] ionic liquid assistance,[6] the hydrolysis reaction,[7] and chemical modification of AB *via* replacing one of its H atoms with other alkali or alkaline earth elements to form metal amidoboranes,[8] to surmount the above-mentioned drawbacks. In particular, by dint of modifying the structure of AB, *i.e.*, replacement of a protonic H atom linked with the N atom of AB with a metal cation to form a series of amidoboranes, the kinetics and thermodynamics of hydrogen release can be significantly improved, along with effective suppression of volatile by-products. With respect to this methodology, a number of recent experimental and theoretical investigations have authenticated the correlation between the ionicity and size of metal cations and the nature of the $NH_2BH_3^-$ bonding in metal amidoboranes, and then determined their individual hydrogen release properties.[9]

In previous reports, studies were mainly focused on the single-metal amidoboranes, *e.g.*, $LiNH_2BH_3$,[10] $NaNH_2BH_3$,[11] KNH_2BH_3,[12] $Ca(NH_2BH_3)_2$,[13,14] $Sr(NH_2BH_3)_2$,[15] and $Y(NH_2BH_3)_3$,[16] which have been successfully synthesized through the reaction between ammonia borane and the relevant metal hydrides or halides. Although these single-metal

[a]*Department of Materials Science, Fudan University, Shanghai, China. E-mail: yuxuebin@fudan.edu.cn; Tel: +86-21-55664581*

[b]*Institute for Superconducting and Electronic Materials, University of Wollongong, North Wollongong, Australia. E-mail: zguo@uow.edu.au*

[c]*School of Mechanical, Materials & Mechatronics Engineering, University of Wollongong, NSW 2522, Australia*

† Electronic supplementary information (ESI) available: Powder XRD of the as-prepared Li_3AlH_6–*n*AB ($n = 4$, 5, and 6) composites and its products, TPD results of the products after hydrogenation, and FTIR spectra of the spent fuels. See DOI: 10.1039/c2ta00697a

amidoboranes exhibited superior hydrogen release properties relative to AB, almost all of them were a source of contamination due to the simultaneous release of ammonia with the hydrogen desorption,[11,13–17] which is a very important issue because a very small amount of ammonia (ppm level) poisons the catalysts for proton exchange membrane (PEM) fuel cells. Fortunately, a small number of mixed-metal amidoboranes, *e.g.*, $LiNa(NH_2BH_3)_2$,[18] $NaMg(NH_2BH_3)_3$,[19] and $Na_2Mg(NH_2BH_3)_4$,[20] have been discovered recently through the solid-phase reaction of ammonia borane with the corresponding mixed-metal hydrides, and these demonstrate that the combination of alkali and alkaline earth metals can effectively promote the reactivity of metal hydrides with AB.[8] Moreover, $M_2Mg(NH_2BH_3)_4$ (M = Na and K) was also prepared by the mechanical reaction of $Mg(NH_2BH_3)_2 \cdot NH_3$ with MH.[21] The thermal stability of the amidoboranes can then be tuned towards favourable dehydrogenation properties. A noteworthy feature is that, due to the incorporation of other structure-stabilizing ligands [$NaNH_2BH_3$], the $Mg(NH_2BH_3)_2$ moiety, which is structurally unstable according to a previous report,[22] is present in some of these mixed-metal amidoboranes, demonstrating the functions of dual-metal ions towards stabilization of unstable complex hydrides, as similarly observed in the synthesis of $MZn(BH_4)_3$ (M = Li, Na), in which the coordination of alkali metals gives rise to the stabilization of $Zn(BH_4)_2$ under ambient conditions.[23] Furthermore, significantly improved hydrogen desorption properties were realized for the mixed-metal amidoboranes in comparison with the mono-metallic amidoboranes, *e.g.*, complete suppression of ammonia was observed for $NaMg(NH_2BH_3)_3$,[19] while there is ~15 mol% ammonia release for $NaNH_2BH_3$. Therefore, the incorporation of alkali metal ions affords an efficient strategy to stabilize amidoboranes which are thermodynamically unstable under ambient conditions, and meanwhile, offers superior hydrogen desorption properties compared with the single-metal amidoboranes.

Based on the above discussion, synthesis based on the milling-induced solid-phase reaction of Li_3AlH_6 with ammonia borane was conducted in this study. This reaction leads to the formation of a mixed alkali metal (Li) and trivalent metal (Al) based metallic amidoborane, which has been proved to possess facile hydrogen release properties without emission of any by-products. More importantly, the as-prepared mixed-metal (Li, Al) amidoborane was shown to be regenerated through treatment with hydrazine in liquid ammonia to some extent, exhibiting an inspiring breakthrough for amidoboranes as future energy carriers.

2 Experimental

2.1 Materials and synthesis

The starting materials, $LiAlH_4$ (97%), LiH (95%), and BH_3NH_3 (97%), were purchased form Sigma-Aldrich and used in as-received form without further purification. Samples of Li_3AlH_6 were synthesized by mixing stoichiometric ratios (1 : 2) of $LiAlH_4$ and LiH powders *via* planetary ball milling (QM-1SP2, 400 rpm, ball to powder ratio of 30 : 1) for 24 h.[24] The mixed product was then loaded into a stainless steel tube under 80 atm H_2 atmosphere, and, in order to improve the purity of the synthesized Li_3AlH_6, the ball-milled products were heated with a ramp of 1 K min^{-1} to 150 °C and annealed at 150 °C overnight. Combinations of Li_3AlH_6 and BH_3NH_3 with various molar ratios were ball milled in the planetary QM-1SP2 mill at 350 rpm under argon for 3 h, using stainless steel spheres with a ball-to-powder weight ratio of 40 : 1. To reduce the heat effect during the ball-milling process, the mill was set to revolve for 30 min in one direction, pause for 30 min, and then revolve in the reverse direction. In the control experiment, mixtures of $LiAlH_4$ and AB were ball milled under identical conditions with different molar ratios. All sample handling was performed in a Ar-filled glove box due to the extreme air-sensitivity of the hydrides.

2.2 Regeneration

The regeneration process was similar to the procedure in a previous report:[2a] in a typical case, the dehydrogenated composites (~100 mg) after heating to 400 °C were suspended in liquid ammonia (~30 mL) at 0 °C in a stainless steel reaction vessel with an internal volume of 75 mL. Hydrazine was acquired from hydrazine sulfate located on dense stainless nets, which were inserted at the top of the stainless steel vessel and used to prevent hydrazine sulfate contamination of the regenerated products. Subsequently, the reaction vessel was sealed and heated to a constant temperature of 40 °C for 3 days, and after that, the vessel was vacuum-dried to remove the residual ammonia for ~12 h, with the remnant of the regenerated products on the bottom.

2.3 Characterization

Simultaneous thermogravimetric analysis (TGA, Netzsch STA 449C) and mass spectrometry (MS, Hidden HPR 20) were simultaneously applied to survey the hydrogen release properties, using a heating rate of 2 °C min^{-1} under dynamic nitrogen with a purge rate of 50 mL min^{-1}. Differential scanning calorimetry (DSC) was performed on a TA Q2000, USA, using a heating rate of 2 °C min^{-1}, with highly pure N_2 as the purge gas. Temperature-programmed desorption (TPD) was also conducted to determine the decomposition behavior of the samples under heating on a semi-automatic Sievert's apparatus connected to the reactor containing the sample (~0.1 g) under 1 atm nitrogen, using a heating rate of 2 °C min^{-1}. Powder X-ray diffraction (XRD, Rigaku D/max 2400) measurements were performed to confirm the phase structure using Cu Kα radiation. Samples were mounted on a glass board in an Ar-filled glove box and then sealed with an airtight hood composed of an amorphous membrane in order to avoid oxidation during XRD measurement. High-resolution X-ray diffraction data were collected by a Mythen-II detector with a wavelength of 0.825 Å at the Powder Diffraction Beamline, Australian Synchrotron. The sample was loaded into a pre-dried 0.7 mm boron–silica glass capillary, and then, the capillary was sealed with vacuum grease in a glove box filled with argon. In order to identify the phase transformations during decomposition, time-resolved *in situ* measurements were conducted using a Cyberstar hot-air blower

to heat the capillary from room temperature to 200 °C, with a constant heating rate of 6 °C min^{-1}. Data were collected with an exposure time of 150 s at every 10 °C step. Fourier transform infrared spectroscopy (FTIR, Magna-IR 550 II, Nicolet) was conducted to confirm the chemical bonds in the samples. Samples were pressed with KBr and then loaded into a sealed chamber for measurement. Solid-state ^{11}B nuclear magnetic resonance (NMR, DSX 300) results were collected using a Doty cross-polarization magic angle spinning (CP-MAS) probe with no probe background. All of the solid samples were spun at 12 kHz, using 4 mm ZrO_2 rotors filled in a purified argon atmosphere glove box. 0.55 μs single-pulse excitation was employed, with repetition time of 1.5 s.

3 Results and discussion

3.1 Phase/structure analysis

The mixed-metal amidoborane composites were prepared by directly ball milling different molar ratios (1 : 4, 1 : 5, and 1 : 6) of lithium hexahydridoaluminate (Li_3AlH_6) with ammonia borane (NH_3BH_3, AB), and further characterized by powder X-ray diffraction (XRD), as shown in Fig. 1 and S1 in the ESI.† According to the high-resolution XRD results (Fig. 1) for the ball-milled Li_3AlH_6 and AB with a molar ratio of 1 : 4, the peaks pertinent to the pristine Li_3AlH_6 and AB precursors have disappeared, and meanwhile, a new set of strong peaks have appeared, suggesting the formation of new crystalline phases from the milling-induced solid-phase interaction. In addition, with different molar ratios of the raw materials, except for the peaks belonging to residual AB due to increased AB content in the composites, identical peak positions were observed, indicative of the formation of the same phase, owing to the reaction between Li_3AlH_6 and AB. Further evidence for the occurrence of the reaction was given by the phenomenon that during the ball-milling process, a gradual pressure increase was detected due to the release of hydrogen, which was subsequently certified as the sole gaseous species *via* mass spectrometry (MS), resulting in approximately 4 equiv. H_2 per Li_3AlH_6 for different molar ratios of Li_3AlH_6 with AB, based on the calculation from the standard gas equation from the known vessel volume for ball milling and the pressure change. These results also revealed that the reaction of Li_3AlH_6 with AB in various molar ratios proceeded by a parallel pathway, resulting in the formation of the mixed-metal amidoborane with the presence of residual raw materials. As a result, rather than the complete consumption of hydrogen atoms in Li_3AlH_6, only four H atoms of Li_3AlH_6 reacted with the $H^{\delta+}$ in NH_3BH_3, leading to the formation of the mixed-metal amidoborane with a chemical composition of $Li_3AlH_2(NH_2BH_3)_4$. Unfortunately, attempts to index the crystal structure of the as-prepared product from the HRXRD pattern failed in the present work, probably due to the poor crystallinity and the possible formation of the mixed-phase of metallic amidoboranes induced during the mechanical preparation process. Apparently, the affinity of $H^{\delta-}$ in Li_3AlH_6 and $H^{\delta+}$ in NH_3 of AB is one of the main driving forces for this solid-phase reaction, accompanied by the release of H_2, comparable to the mechanism for the formation of other metallic amidoboranes.[10–15,18–20]

In order to acquire better information on the reaction products derived from Li_3AlH_6 and AB, chemical bonds of the samples were detected by solid-state ^{11}B NMR and FTIR spectra. The ^{11}B NMR results (Fig. 2) exhibit the dominant BH_3 resonance centered at −26.3 ppm from neat AB in accordance with previous reports,[25] while the resonance for the BH_3 group shifts downfield to around −20.1 ppm in the post-milled Li_3AlH_6–4AB sample, similar to the trends for the previously reported metallic amidoboranes, due to the incorporation of metal cations with higher electron densities, leading to the formation of stronger donor complexes with borane.[10a,19,26] Moreover, the fact that only one principal peak is observed for the thus-synthesized product from the mechanically milled Li_3AlH_6–4AB suggests the same chemical environment for all the boron sites. Additionally, with increasing amounts of AB in the raw

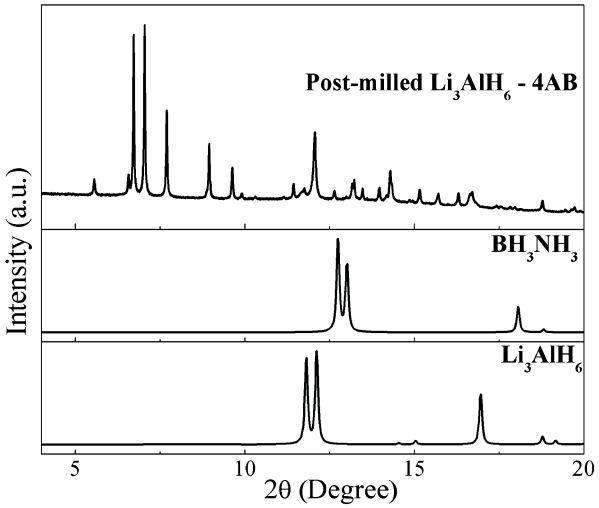

Fig. 1 High-resolution X-ray diffraction pattern of the post-milled Li_3AlH_6–4AB composite, with the patterns of pristine AB and Li_3AlH_6 included for comparison.

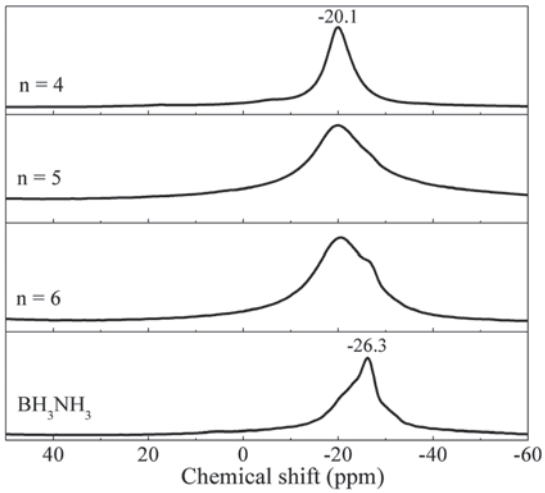

Fig. 2 Solid-state ^{11}B NMR spectra of the as-prepared Li_3AlH_6–*n*AB ($n = 4$, 5, and 6) composites, including pure AB for comparison.

materials, the line width for the resonance of the BH_3 moiety is broadened, instead of splitting into two peaks attributable to the thus-synthesized mixed-metal amidoborane and the residual AB, respectively, due to the relatively low resolution of solid-state NMR spectra. Furthermore, the resonance for the mobile phase of AB,[25,27] which has a high reactivity compared to its parent AB, was also observed as a shoulder on the primary peak belonging to the as-prepared mixed-metal amidoborane for the sample with a molar ratio of AB : Li_3AlH_6 = 6 : 1, indirectly demonstrating the partial reaction between Li_3AlH_6 and AB rather than the complete consumption of $H^{\delta-}$ in Li_3AlH_6 during the reaction process.[20] Analogous to the NMR results, after replacing $H^{\delta+}$ in NH_3 of AB by metal cations, significant bonding structure changes were observed in the FTIR spectra of the resultant products in comparison with their raw substrates, *i.e.*, Li_3AlH_6 and AB. The FTIR results (Fig. 3) show that identical peaks were observed for all the thus-prepared samples, even though there were different molar ratios of Li_3AlH_6 to AB. The peak positions of the N–H and B–H bonds at around 3150–3350 cm^{-1} and 2200–2400 cm^{-1}, respectively, in stretching modes are comparable with those of pure ammonia borane, while the peaks of the bending modes for N–H bonds and B–H bonds are split into two peaks and three peaks, respectively, indicating the complexity of the bonding structure, as well as the reduced structural symmetry of the as-prepared compounds compared with AB, which is also observed for other monometallic amidoboranes[16,17] and $NaMg(NH_2BH_3)_3$.[19] In addition, the peak at around 864 cm^{-1} assigned to the bending mode of the LiAl–H bond was present,[28] providing further evidence for the validity of the incomplete depletion of H atoms when Li_3AlH_6 reacts with AB during the ball-milling process. Interestingly, a weak band at around 618 cm^{-1}, attributed to the stretching mode of the Al–N bond, is present in all the post-milled samples, which directly confirms the interaction between Li_3AlH_6 and AB during ball milling, leading to substitution for hydridic hydrogen by the $NH_2BH_3^-$ group to form the mixed-metal amidoborane. Moreover, the strong band at 1380 cm^{-1} corresponds to the combination of B–N stretching and Al–N stretching resonances. The increase in the relative intensity of this peak after ball milling compared with other peaks may be attributed to the formation of Al–N bonds due to the reaction of Li_3AlH_6 with AB.

With reference to the reaction of $LiAlH_4$ with ammonium halides,[29] *e.g.*, NH_4Cl, accompanied by violent hydrogen release resulting from the combination of 3 equiv. Al–H bonds and 3 equiv. N–H bonds, the reaction of $LiAlH_4$ with AB has been attempted in an effort to synthesize lithium aluminum amidoboranes. However, attempts to conduct this reaction have failed due to the significant release of boric byproducts (*i.e.*, diborane and borazine) together with hydrogen desorption, even during a hand milling process, resulting in the formation of amorphous products and Al (Fig. S2†). Therefore, the incorporation of LiH into $LiAlH_4$, *i.e.*, the formation of Li_3AlH_6, plays an important role in stabilizing the reaction between Al–H bonds and N–H bonds, indicating the crucial functionality of the alkali metal in tuning the reactivity of metal hydrides with AB.

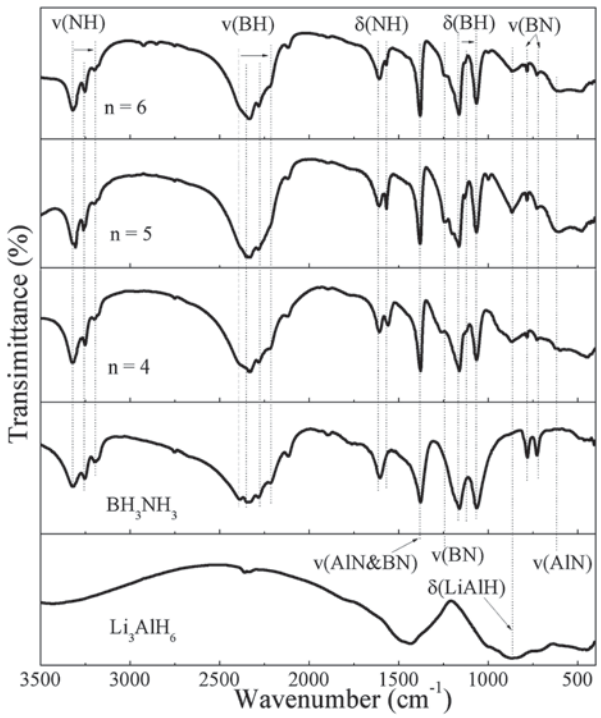

Fig. 3 FTIR spectra of the as-prepared Li_3AlH_6–*n*AB (*n* = 4, 5, and 6) composites, including spectra of pristine AB and as-prepared Li_3AlH_6 for comparison.

3.2 Hydrogen desorption properties

For comparison with AB, the thermal decomposition performances of the post-milled Li_3AlH_6–*n*AB (*n* = 4, 5, and 6) were investigated by employing mass spectrometry (MS), and the results are shown in Fig. 4 and S3.† The effective suppression of boric impurities during the decomposition of ammonia borane, *i.e.*, borazine and diborane, was successfully achieved in the as-prepared Li_3AlH_6–*n*AB (*n* = 4, 5, and 6) composites. Moreover, the evolution of ammonia was reduced to levels below the detection threshold of mass spectrometry in the cases of the Li_3AlH_6–*n*AB (*n* = 4 and 5) composites, and only a slight amount of ammonia was released for the Li_3AlH_6–6AB composite, indicating significantly improved hydrogen release purity for the Li_3AlH_6–*n*AB composites in comparison with the neat AB. Additionally, compared with the dehydrogenation of neat AB with only two dominant peaks at around 118 °C and 160 °C,[30] multiple hydrogen release peaks appear during the decomposition of the Li_3AlH_6–*n*AB (*n* = 4, 5, and 6) composites, which are similar to the hydrogen release process of other reported metallic amidoboranes,[10c,15–20] suggesting distinct mechanisms for the thermolysis process causing hydrogen desorption. Specifically, Li_3AlH_6–4AB starts to release hydrogen at around 82 °C, with a two-step dehydrogenation process that peaks at 99.7 °C and 148.9 °C, respectively, much lower than that for pure AB. In the case of the Li_3AlH_6–5AB composite, the onset hydrogen release temperature further decreases to around 56 °C, approximately 26 °C and 49 °C lower than for the Li_3AlH_6–4AB and the neat AB (~105 °C for BH_3NH_3), respectively. Meanwhile, the first hydrogen evolution peak is reduced to

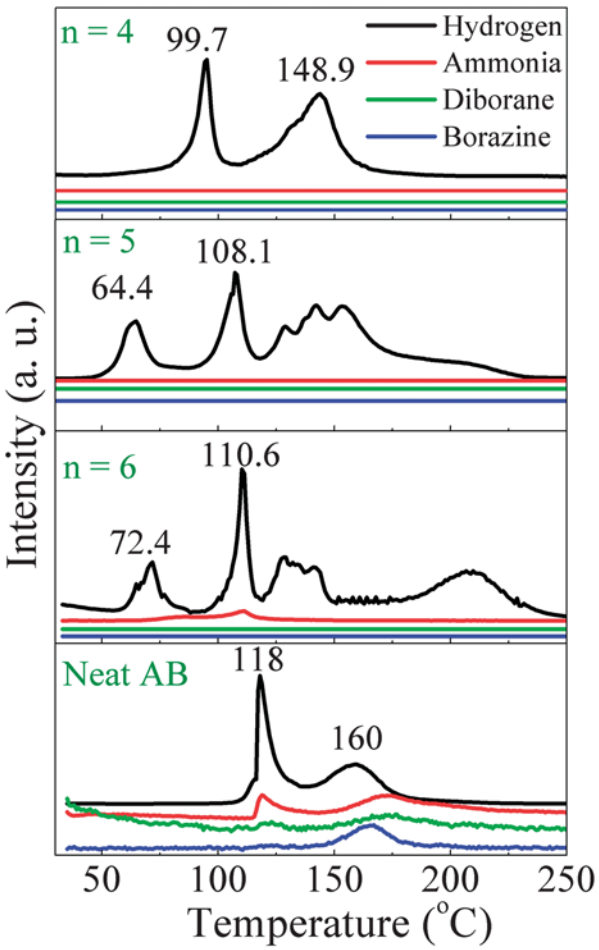

Fig. 4 MS spectra of the as-prepared Li_3AlH_6–*n*AB (*n* = 4, 5, and 6) composites with a heating rate of 2 °C min^{-1} under 1 atm dynamic N_2 atmosphere, including neat AB for comparison.

64.4 °C, a remarkable decrease, even in comparison with lithium amidoborane (~91 °C for $LiNH_2BH_3$), while the second hydrogen evolution peak is centered at 108.1 °C. Thereafter, multiple hydrogen release peaks are present in the temperature range from 120 °C to 180 °C, illustrating its complicated decomposition mechanism. Comparable results were also observed for the post-milled Li_3AlH_6–AB composite with a molar ratio of 1 : 6, with the first hydrogen release peak at 72.4 °C and a following broad peak at temperatures from 180 °C to 240 °C. Some evolution of ammonia was identified, however, during the dehydrocoupling process ranging from 67 °C to 132 °C. Moreover, it is noteworthy that the as-synthesized Li_3AlH_6–*n*AB composites are free from volume expansion, which is one of the major problems suffered by AB during hydrogen desorption. As per the above-mentioned results, Li_3AlH_6–*n*AB composites exhibit substantially enhanced hydrogen release properties compared with pure ammonia borane, including the effective suppression of volatile boric impurities and much lower hydrogen release temperatures.

Thermogravimetric analysis (TGA) combined with volumetric temperature programmed desorption (TPD) measurements were subsequently performed to quantitatively identify the capacity and purity of hydrogen release from the Li_3AlH_6–*n*AB (*n* = 4, 5, and 6) composites. As shown in Fig. 5, Li_3AlH_6–4AB presents a two-step decomposition, with 3.85 wt% weight loss for the first step in the region of 80–110 °C and 6.25 wt% for the second step from 110 °C to 175 °C, in good correspondence with the volumetric results (~3.25 equiv. and ~5.3 equiv. for the first and second dehydrogenation steps, respectively), demonstrating the release of hydrogen with high purity, as indicated in the MS spectra. This result indicates the superior effects of the as-prepared mixed-metal (Li, Al) amidoborane on suppressing ammonia release compared with other dual-metal amidoboranes.[18–20] With regard to the Li_3AlH_6–5AB composite, the total weight loss is around 12 wt% over the whole decomposition, corresponding to 12 equiv. H_2, which is also consistent with the volumetric results (~12.32 equiv.), again confirming the release of high-purity hydrogen in this composite. Thus far, multiple volatile by-products due to the decomposition of residual ammonia borane can be effectively suppressed by the presence of the thus-synthesized mixed-metal amidoborane in a theoretical molar ratio of 1 : 1. By contrast, the TGA results for the Li_3AlH_6–6AB sample give a weight loss of 13.6 wt%, corresponding to approximately 15.7 equiv. H_2, while only 14.27 equiv. gas is evolved according to the volumetric results,

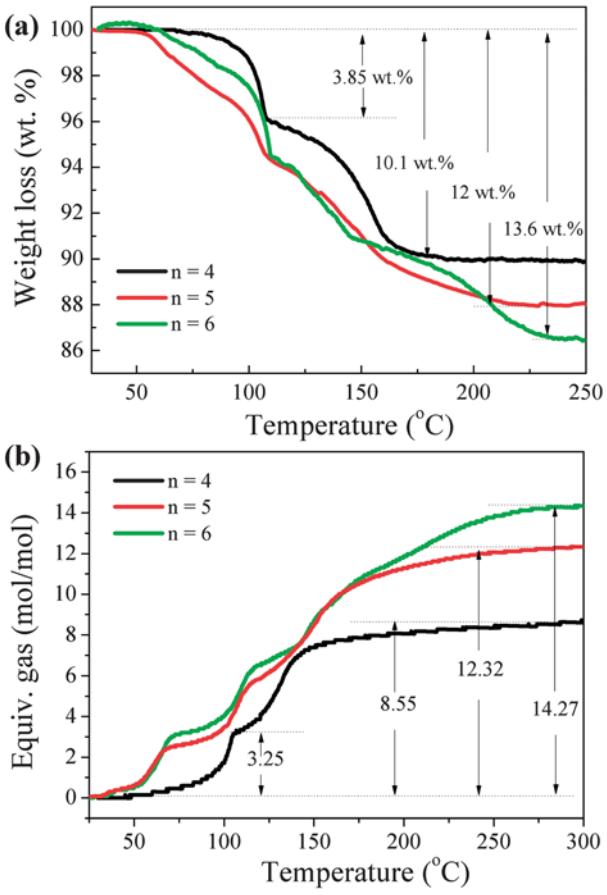

Fig. 5 (a) TGA and (b) volumetric results for the decomposition of the post-milled Li_3AlH_6–*n*AB (*n* = 4, 5, and 6) composites at a heating rate of 2 °C min^{-1} under 1 atm N_2 atmosphere.

suggesting the presence of by-products during the dehydrogenation process, *i.e.*, ammonia, as detected by the MS spectra. Given that ammonia is the only by-product in conjunction with the dehydrogenation during its decomposition, on the basis of the TGA and volumetric results, the H_2 content evolved during decomposition of Li_3AlH_6–6AB composite was calculated to be 98.7 mol% (89.7 wt%), reflecting the fact that the thus-synthesized mixed-metal amidoborane not only exhibits superior hydrogen release properties, but also plays an important role in suppressing the release of volatile side products during the decomposition of residual ammonia borane, *e.g.*, ammonia, borazine, and diborane.

Insights into the dehydrogenation kinetics of Li_3AlH_6–*n*AB composites were gained by applying the volumetric desorption measurements at different temperatures. As displayed in Fig. 6, with increasing operating temperature, faster kinetics is yielded for the Li_3AlH_6–*n*AB composites. Li_3AlH_6–4AB released 4 wt% hydrogen at 90 °C and 4.2 wt% hydrogen at 100 °C within 100 min. Upon further elevating the temperature to 120 °C and 130 °C, hydrogen capacities of ~7 wt% and 9.3 wt% can be reached, respectively, in 200 min, after a drastic hydrogen evolution within several minutes. In the case of Li_3AlH_6–5AB, enhanced hydrogen release kinetics was present above 90 °C compared with the Li_3AlH_6–4AB. In particular, at 120 °C, around 8 wt% hydrogen was released within only 45 min. With respect to the Li_3AlH_6–6AB, further improved dynamic performance was exhibited, especially at relatively low operating temperatures in comparison with the Li_3AlH_6–5AB. For instance, 5 wt%, 6 wt%, and 7 wt% hydrogen evolution could be accomplished at temperatures of 80 °C, 90 °C, and 110 °C within 200 min, respectively, which are around 1 wt% higher than for Li_3AlH_6–5AB under the same conditions. For a quantitative evaluation of the kinetic properties related to hydrogen release, the apparent activation energies were calculated from various isothermal dehydrogenation results *via* linear Arrhenius plots of ln *k*, where *k* is the rate constant, as a function of 1/*T*. Fig. 6(d) displays the details for calculation of apparent activation energies. It gives activation energies of approximately 32.6 kJ mol^{-1}, 27.7 kJ mol^{-1}, and 12.8 kJ mol^{-1} for Li_3AlH_6–*n*AB composites with n = 4, 5, and 6, respectively, indicating more favourable hydrogen release properties with increasing AB content in the raw materials.

3.3 Decomposition mechanism

Because the hydrogen release for this system is mainly due to the combination of hydridic hydrogen with protonic hydrogen, *i.e.*, $H^{\delta+}$ linked to the N atom with $H^{\delta-}$ linked to the B or Al atom, the decomposition of the Li_3AlH_6–*n*AB (n = 4, 5, and 6) composites is determined to be exothermic as confirmed by the DSC results (Fig. 7), which are similar to the behaviour of other metallic amidoboranes.[10–20] In particular, upon decomposition, Li_3AlH_6–4AB exhibits a small exothermic peak at around 57 °C, which is proposed to be the reaction of residual Li_3AlH_6 (Fig. 1) with ammonia borane, and then a major hydrogen release peak at around 100 °C, followed by some small peaks in the region of 116–150 °C, consistent with the hydrogen release results from the mass spectra. With the aim of unravelling the relatively intricate decomposition mechanism for the Li_3AlH_6–*n*AB (n = 4, 5, and 6) composites according to the MS results, *in situ* high-resolution X-ray diffraction was performed to survey the phase transformation during decomposition of the thus-synthesized mixed-metal amidoborane during heating. As shown in Fig. 8, no structural change occurred before 80 °C, but upon further heating, all the peaks belonging to the synthesized mixed-metal amidoborane were significantly weakened at ~80 °C and disappeared at around 100 °C, indicating that the onset of hydrogen desorption from the mixed-metal amidoborane starts from ~80 °C, which is consistent with the MS results. After heating the sample to 200 °C, the mixed-metal amidoborane decomposed to form an amorphous state, which accounts for the formation of N–B chain oligomerization concurrent with the release of hydrogen during the decomposition of the metal amidoboranes.[9b] Additionally, a recent study by Pruski's group[31] found that upon heating, the interaction of a physical mixture of Li_3AlH_6 and AB with a molar ratio of 1 : 3 formed $LiNH_2BH_3$

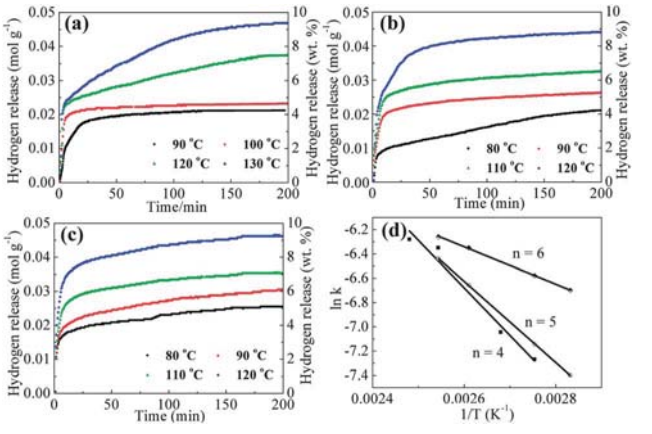

Fig. 6 Isothermal volumetric measurements of hydrogen release from Li_3AlH_6–*n*AB composites when n = 4 (a), 5 (b), and 6 (c) at different temperatures, and (d) Arrhenius plots of the temperature-dependent rate data.

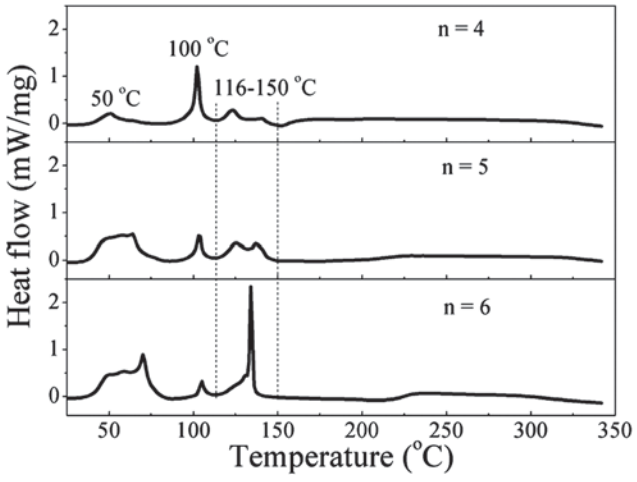

Fig. 7 Differential scanning calorimetry results for Li_3AlH_6–*n*AB (n = 4, 5, and 6) composites under a heating rate of 2 °C min^{-1} in 1 atm N_2 atmosphere.

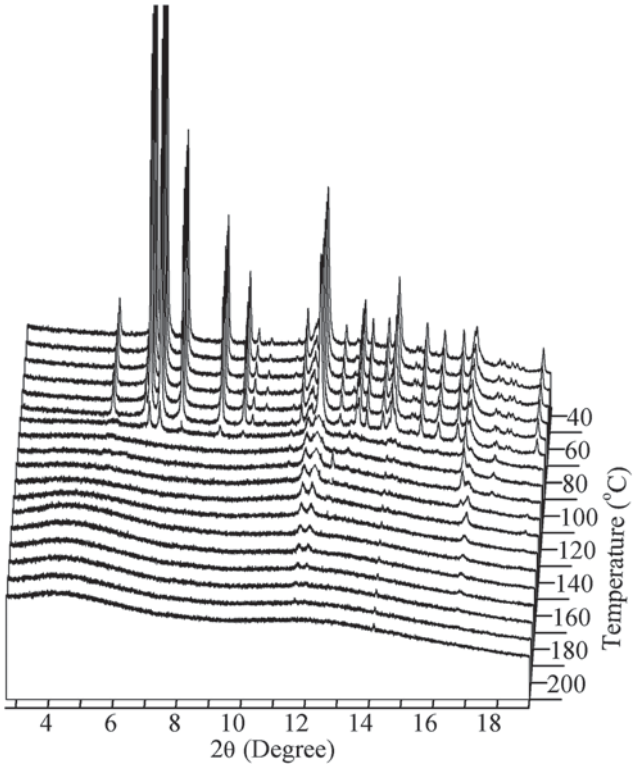

Fig. 8 Selected range of the *in situ* high-resolution XRD patterns for the post-milled Li_3AlH_6–4AB composites at different temperatures.

adducted with AB, which mainly accounts for the accelerated formation of branched polyaminoborane and hydrogen release, with the generation of AlH_3 and LiH as intermediate compounds. However, the post-milled mixtures of Li_3AlH_6 and AB in the present work exhibit a significantly different mechanism from the physical mixture of Li_3AlH_6 and AB, as no intermediate compounds, *e.g.*, LiH and AlH_3, were detected in the *in situ* XRD results for the decomposition of the composite with a molar ratio of 1 : 4, and the XRD results for the dehydrogenated products identify no formation of metallic Al (Fig. 8 and S4†). The distinct pathway for hydrogen release may originate from the fact that temperature is an important factor for both the interaction between Li_3AlH_6 and AB and the subsequent decomposition, due to their exothermic nature.

With respect to Li_3AlH_6–5AB and Li_3AlH_6–6AB, exothermic peaks for hydrogen release at temperatures comparable with the MS results for hydrogen evolution were also detected. By contrast, compared with the post-milled Li_3AlH_6–4AB sample, due to the presence of residual AB of the mobile phase in the raw materials for the Li_3AlH_6–*n*AB (n = 5 and 6) composites (Fig. 2), the onset dehydrogenation temperature from the $n = 5$ and 6 composites lowered to around 56 °C, and the hydrogen release peaks appeared before the onset hydrogen release temperature of the post-milled Li_3AlH_6–4AB sample, as demonstrated by the MS and TGA results. XRD patterns of the Li_3AlH_6–*n*AB ($n = 5$ and 6) composites after heating to 90 °C are presented in Fig. S5† so that the phase transformation due to the presence of residual AB originating from hydrogen desorption at temperatures below 90 °C can be ascertained. Interestingly, the diffraction peaks of the thus-synthesized mixed-metal amidoborane can still be clearly identified in the post-heated samples, although with weakened identity, and the peaks indexed to residual AB have disappeared, providing direct evidence for the participation of surplus AB of the mobile phase in the hydrogen desorption at temperatures ranging from 56 to 90 °C. In addition, based on the TGA and TPD results, more than 2 equiv. H_2, which is the theoretically releasable hydrogen capacity below 200 °C,[10a] was detached. Therefore, the hydrogen release below 90 °C is possibly derived from not only the decomposition of residual AB, but also the cooperative mechanism of AB with the as-synthesized mixed-metal amidoborane. The interaction of amidoboranes with AB, although in the room temperature phase, is also evidenced by the decomposition of the $LiNH_2BH_3 \cdot NH_3BH_3$ system, leading to significantly improved hydrogen release properties due to the combination of N–H bonds with B–H bonds between the $LiNH_2BH_3$ moiety and the BH_3NH_3 moiety, which forms polyaminoborane-like products of an amorphous nature.[30] The synergistic effects of the interaction of AB with $LiNH_2BH_3$ is free of any induction period, which is attributed to the disruption of dihydrogen bonds and the slow formation of $[NH_3BH_2NH_3]^+[BH_4]^-$ (DADB), which is surmised to be a key reactive species for H_2 liberation from AB.[32] It is believed that the reaction of the as-synthesized mixed-metal amidoborane with the mobile phase of AB resembles the interaction of $LiNH_2BH_3$ with AB, resulting in improved hydrogen release properties with the formation of amorphous products and the preservation of residual mixed-metal amidoborane, as indicated in the XRD patterns (Fig. S5†). Furthermore, due to the decrease and/or weakening of dihydrogen bonds in the mobile AB phase,[27] which results in higher reactivity relative to the room temperature phase of AB, the energy barrier for the combination of N–H bonds with B–H bonds between metallic amidoborane and AB in the mobile phase is reduced. It, therefore, gives rise to lower onset and peak temperature of hydrogen release for the post-milled Li_3AlH_6–*n*AB (n = 5 and 6) composites compared with $LiNH_2BH_3 \cdot NH_3BH_3$,[30] in which the reaction of $LiNH_2BH_3$ with the room temperature phase of AB leads to the release of hydrogen. In addition, it should be noted that, as indicated from MS and DSC results, the participation of the AB in the mobile phase in the decomposition of the thus-synthesized mixed-metal amidoborane results in a more intricate dehydrogenation pathway for the post-milled Li_3AlH_6–*n*AB ($n = 5$ and 6) composites compared with the Li_3AlH_6–4AB sample. Obviously, similar to the decomposition mechanism of other metallic amidoboranes, the dihydrogen bonding network and the metal ion assisted hydride transfer are of significant importance for the substantially improved hydrogen release properties compared with ammonia borane.[9a]

Due to the limited characterization of the materials in the amorphous state that is possible by other techniques, further exploration of the post-heated samples was provided *via* NMR and FTIR spectra to monitor the chemical environments of B and N, as shown in Fig. 9. The formation of sp^2-hybridized boron and BN_3H, ranging from −10 to 30 ppm and centered at

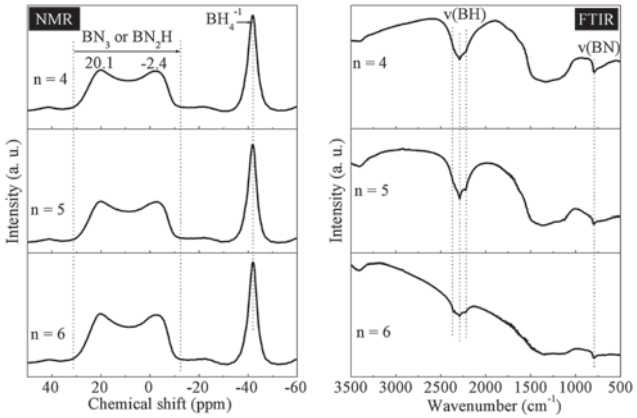

Fig. 9 Solid-state ^{11}B NMR and FTIR spectra of Li_3AlH_6–*n*AB (n = 4, 5, and 6) composites upon heating to 350 °C with a heating rate of 2 °C min^{-1}.

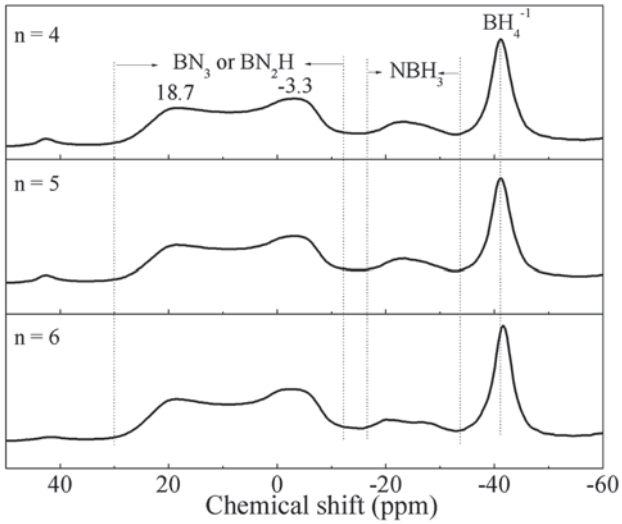

Fig. 10 Solid-state ^{11}B NMR spectra of Li_3AlH_6–*n*AB (n = 4, 5, and 6) composites after regeneration from the spent fuels.

20.1 and −2.4 ppm, was observed in the ^{11}B NMR results, in tandem with the fact that most N–H stretches disappeared from the FTIR spectra in the post-heated samples, which are reminiscent of the dehydrogenated products of other amidoboranes,[10–20] further demonstrating that the combination of hydridic $H^{\delta+}$ and protonic $H^{\delta-}$ in general accounts for the hydrogen desorption from Li_3AlH_6–*n*AB (n = 4, 5, and 6) composites. Interestingly, the presence of an unsaturated boron structure offers significant potential for the regeneration of hydrogen-depleted composites using hydrazine as the reductant in liquid ammonia.[2a] In addition to that, a principal signal at −41 ppm, corresponding to the BH_4^- moiety in the NMR spectra, and B–H stretches in the FTIR spectra are present in the dehydrogenated samples, while no peaks indexed to metal borohydrides are present in the XRD results, indicating the amorphous state of the thus-formed borohydrides. Similar phenomena were observed in the products from the decomposition of lithium amidoborane.[10a]

3.4 Regeneration

The practical application of Li_3AlH_6–*n*AB composites lies not only in the hydrogen desorption performance, but also in the hydrogenation conditions of the spent fuel. Efforts to restore the spent fuels were impractical *via* direct solid–gas reaction, however, due to the exothermicity of the hydrogen release reaction. On the other hand, inspired by recent advances in efficient regeneration of AB from the highly unsaturated sp^2-hybridized boron structure in polyborazylene, which is the predominant environment for boron after dehydrogenation to 350 °C for Li_3AlH_6–*n*AB composites, as shown in Fig. 9, chemical hydrogenation, by treating the decomposed products with hydrazine as the reductant in liquid ammonia, was attempted. To prove the feasibility of this method, firstly, solid-state ^{11}B NMR spectra were employed to detect the environmental changes experienced by boron in the regenerated products. From the NMR results (Fig. 10), it can be seen that, after regeneration of the dehydrogenated Li_3AlH_6–*n*AB composites, a broad peak belonging to NBH_3, which was also present in the original samples (Fig. 2), appears. Nevertheless, the presence of unreacted sp^2-hybridized boron and the BN_3H analogue confirms the partial transformation of the unsaturated boron structure to the NBH_3 analogue species under the reducing action of hydrazine in liquid ammonia. By contrast with the dehydrogenated products, the intensity ratio between the relative downfield region (centered at 20.1 ppm in the dehydrogenated products and 18.7 ppm in the regenerated products) and the relative upfield region (centered at −2.4 ppm in the dehydrogenated products and −3.3 ppm in the regenerated products) was reduced for the regenerated sample, suggesting that the more unsaturated boron structure there is, the more readily it is hydrogenated. This is mainly attributed to the fact that the position of the peak in the downfield region more closely resembles that of the polyborazylene from the decomposition of AB at ~26 ppm.[33] Moreover, in comparison with the resonance of the freshly ball-milled counterparts, the regions of the NBH_3 resonance for the regenerated composites are substantially broader, indicating that more complicated environments for boron may exist in the regenerated samples. Furthermore, FTIR (Fig. 11) was employed to monitor the bonding changes in the regenerated products. Strong peaks pertinent to the characteristic resonance of B–H bonds, corresponding to the distinct peaks of BH_4 and BH_3 fragments in the NMR spectra, were obtained. However, only weak peaks for N–H bonds were observed at the identical positions, suggesting that there are similar chemical environments for N–H bonds after regeneration. Based on the mechanism for hydrogenation from polyborazylene to ammonia borane, the BH_3 moiety is first formed by combination with residual N_2H_4, and then replaced by NH_3, leading to the formation of AB.[2a] In contrast to AB, in which the BH_3 from the BN_3 or BN_3H groups reduced by hydrazine during the process of reduction of decomposed Li_3AlH_6–*n*AB composite, substitution is more difficult, probably due to the presence of metal cations, which may interact with the resultant polymeric BN_3 or BN_3H from dehydrogenation leading to strengthened B–N bonds compared with pure

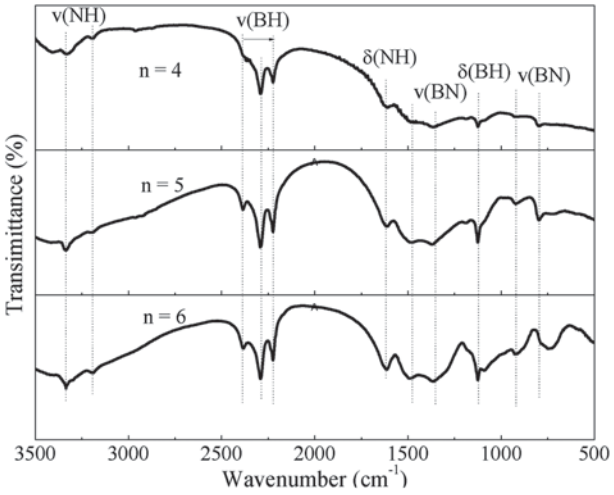

Fig. 11 FTIR spectra of Li_3AlH_6–*n*AB (n = 4, 5, and 6) composites after regeneration from the spent fuels.

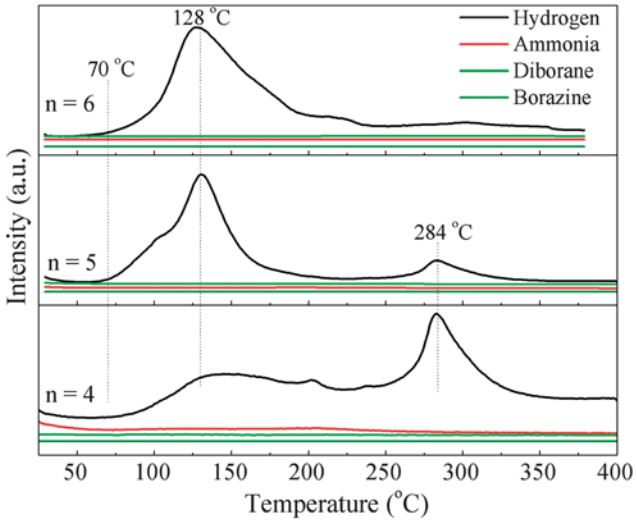

Fig. 12 MS spectra of the Li_3AlH_6–*n*AB (n = 4, 5, and 6) composites after regeneration from the spent fuels.

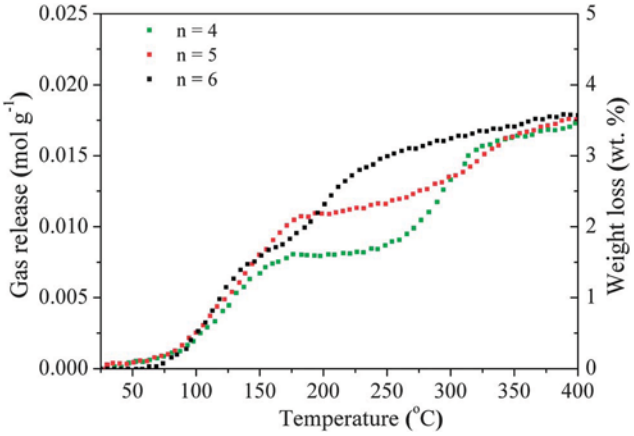

Fig. 13 TPD results for the decomposition of Li_3AlH_6–*n*AB (n = 4, 5, and 6) composites after regeneration from the spent fuels.

polyborazylene formed from the decomposition of ammonia borane. Therefore, the chemical regeneration of the spent fuel from Li_3AlH_6–*n*AB composites upon treatment with hydrazine in liquid ammonia gives rise to partial regeneration in comparison with the 95% yield for the regeneration of AB from polyborazylene. Additionally, with increasing AB content in the raw materials, the intensity of the N–H bonds in the related products after regeneration increases, suggesting that more N–H bonds are present. It is worth noting that, due to the presence of excess AB in the Li_3AlH_6–*n*AB (n = 5 and 6) composites, the possible regeneration of the NH_3 group in AB may partially account for the presence of some N–H bonds in the related products after regeneration.

Further evidence for the successful regeneration of the dehydrogenated Li_3AlH_6–*n*AB composites was obtained by employing MS spectra and volumetric measurements. Impressively, hydrogen is the exclusive product detectable by MS from the regeneration products (Fig. 12), even for the regenerated Li_3AlH_6–6AB sample, in which the decomposition of the freshly milled composite shows ammonia as a by-product coupled with the main release of hydrogen, as displayed in Fig. 4. Moreover, in contrast to the as-milled samples, all the regenerated composites start to release hydrogen at approximately 70 °C, with the first peak centered at around the same temperature of 128 °C, which is a little higher than the freshly ball-milled composites. This resemblance is probably due to their comparable H environments, connected to B and N, as indicated by the FTIR and NMR spectra for the samples after regeneration. According to the TPD results (Fig. 13), all the regenerated Li_3AlH_6–*n*AB (n = 4, 5, and 6) composites show a dehydrogenation capacity of around 3.5 wt%, corresponding to an approximate 35%, 30%, and 26% regeneration yield for the post-milled Li_3AlH_6–*n*AB composites with n = 4, 5, and 6, respectively. Due to the partial regeneration of unsaturated B–N bonds and formation of stable BH_4 groups during decomposition, the second dehydrogenation capacity of the regenerated Li_3AlH_6–6AB was decreased to less than 1.5 wt% (Fig. S6†), only accounting for around 11% regeneration yield.

From Fig. 12 and 13, it can be seen that the samples after hydrogenation exhibit various traits, with distinct two-step dehydrogenation for the regenerated Li_3AlH_6–*n*AB (n = 4, and 5) composites, while the regenerated Li_3AlH_6–6AB shows superior dehydrogenation kinetics at relatively lower temperatures. According to the IR spectra, the N–H bond content in the regenerated products increases with increasing content of ammonia borane, consequently leading to an excess of B–H bonds in the regenerated samples from Li_3AlH_6–*n*AB (n = 4 and 5) composites in comparison with Li_3AlH_6–6AB, in which the decomposition accounts for the 2nd step hydrogen desorption upon further heating. This can be further confirmed by the disappearance of N–H bonds in the rehydrogenated samples from the Li_3AlH_6–4AB composite after heating to 250 °C and the presence of weakened B–H bonds due to their consumption in the reaction with N–H bonds, as shown in Fig. S7.† Indeed, even after dehydrogenation to 400 °C, B–H bonds are still present,

which is attributable to the presence of relatively stable BH_4^- groups like those in alkali metal borohydrides.[34]

4 Conclusion

By incorporation of alkali metal, alkali metal (Li) and trivalent metal (Al) based metallic amidoborane was successfully prepared. The significantly enhanced hydrogen release properties at low temperature, together with the effective suppression of volatile by-products, make it a promising hydrogen storage candidate. It has been shown through volumetric measurements that this novel compound is able to release 9 wt% H_2 at the temperature of 130 °C within 200 min. Furthermore, promotion of hydrogen release from AB through its interaction with the thus-prepared mixed-metal amidoborane was found, including effective suppression of boric by-products and improved hydrogen release kinetics compared with the components, *i.e.*, over 9 wt% H_2 released at 120 °C within 200 min. The products after regeneration are able to release around 3.5 wt% H_2 corresponding to a 35% regeneration yield for the post-milled Li_3AlH_6–4AB composite. These advances may open up the possibility of exploring amidoboranes as a series of practical hydrogen storage materials. In order to commercialize this route using amidoboranes as hydrogen carriers, however, more issues, especially for the enhancement of recyclable hydrogen capacity, still need to be addressed in the future.

Acknowledgements

This work was partially supported by the Ministry of Science and Technology of China (2010CB631302), the National Natural Science Foundation of China (Grant no. 51071047, 21271046), the PhD Programs Foundation of the Ministry of Education of China (20110071110009) and the Science and Technology Commission of Shanghai Municipality (11JC1400700, 115207011100). Z. Guo acknowledges financial support from the Australian Research Council (ARC) discovery project (grant number DP1094261). Part of this research was undertaken on the Powder Diffraction Beamline at the Australian Synchrotron, Victoria, Australia. The authors also would like to thank Dr Tania Silver for critical reading of the manuscript.

Notes and references

1 (*a*) T. K. A. Hoang and D. M. Antonelli, *Adv. Mater.*, 2009, **21**, 1787–1800; (*b*) L. Schlapbach and A. Zuttel, *Nature*, 2001, **414**, 353–358; (*c*) S. Orimo, Y. Nakamori, J. R. Eliseo, A. Züttel and C. M. Jensen, *Chem. Rev.*, 2007, **107**, 4111–4132.

2 (*a*) A. D. Sutton, A. K. Burrell, D. A. Dixon, E. B. Garner III, J. C. Gordon, T. Nakagawa, K. C. Ott, J. P. Robinson and M. Vasiliu, *Science*, 2011, **331**, 1426–1429; (*b*) B. L. Davis, D. A. Dixon, E. B. Garner, J. C. Gordon, M. H. Matus, B. Scott and F. H. Stephens, *Angew. Chem., Int. Ed.*, 2009, **48**, 6812–6816; (*c*) A. D. Sutton, B. L. Davis, K. X. Bhattacharyya, B. D. Ellis, J. C. Gordon and P. P. Power, *Chem. Commun.*, 2010, **46**, 148–149.

3 (*a*) A. Staubitz, A. P. M. Robertson and I. Manners, *Chem. Rev.*, 2010, **110**, 4079–4124; (*b*) W. Grochala and P. P. Edwards, *Chem. Rev.*, 2004, **104**, 1283–1315.

4 (*a*) L. Li, X. Yao, C. Sun, A. Du, L. Cheng, Z. Zhu, C. Yu, J. Zou, S. C. Smith, P. Wang, H.-M. Cheng, R. L. Frost and G. Q. Lu, *Adv. Funct. Mater.*, 2009, **19**, 265–271; (*b*) A. Gutowska, L. Li, Y. Shin, C. M. Wang, X. S. Li, J. C. Linehan, R. S. Smith, B. D. Kay, B. Schmid, W. Shaw, M. Gutowski and T. Autrey, *Angew. Chem., Int. Ed.*, 2005, **44**, 3578–3582; (*c*) S. Sepehri, B. B. García and G. Cao, *Eur. J. Inorg. Chem.*, 2009, **2009**, 599–603; (*d*) S. F. Li, Y. H. Guo, W. W. Sun, D. L. Sun and X. B. Yu, *J. Phys. Chem. C*, 2010, **114**, 21885–21890; (*e*) T. Zhang, X. Yang, S. Yang, D. Li, F. Cheng, Z. Tao and J. Chen, *Phys. Chem. Chem. Phys.*, 2011, **13**, 18592–18599; (*f*) T. K. Nielsen, F. Besenbacher and T. R. Jensen, *Nanoscale*, 2011, **3**, 2086–2098.

5 (*a*) T. He, Z. T. Xiong, G. T. Wu, H. L. Chu, C. Z. Wu, T. Zhang and P. Chen, *Chem. Mater.*, 2009, **21**, 2315–2318; (*b*) B. L. Conley, D. Guess and T. J. Williams, *J. Am. Chem. Soc.*, 2011, **133**, 14212–14215; (*c*) S. B. Kalidindi, J. Joseph and B. R. Jagirdar, *Energy Environ. Sci.*, 2009, **2**, 1274–1276.

6 (*a*) M. E. Bluhm, M. G. Bradley, R. Butterick, U. Kusari and L. G. Sneddon, *J. Am. Chem. Soc.*, 2006, **128**, 7748–7749; (*b*) D. W. Himmelberger, C. W. Yoon, M. E. Bluhm, P. J. Carroll and L. G. Sneddon, *J. Am. Chem. Soc.*, 2009, **131**, 14101–14110.

7 (*a*) X. B. Zhang, S. Han, J. M. Yan, M. Chandra, H. Shioyama, K. Yasuda, N. Kuriyama, T. Kobayashi and Q. Xu, *J. Power Sources*, 2007, **168**, 167–171; (*b*) D. Sun, V. Mazumder, O. n. Metin and S. Sun, *ACS Nano*, 2011, **5**, 6458–6464.

8 P. Wang, *Dalton Trans.*, 2012, **41**, 4296–4302.

9 (*a*) A. T. Luedtke and T. Autrey, *Inorg. Chem.*, 2010, **49**, 3905–3910; (*b*) D. Y. Kim, H. M. Lee, J. Seo, S. K. Shin and K. S. Kim, *Phys. Chem. Chem. Phys.*, 2010, **12**, 5446–5453.

10 (*a*) Z. T. Xiong, C. K. Yong, G. T. Wu, P. Chen, W. Shaw, A. Karkamkar, T. Autrey, M. O. Jones, S. R. Johnson, P. P. Edwards and W. I. F. David, *Nat. Mater.*, 2008, **7**, 138–141; (*b*) C. Wu, G. Wu, Z. Xiong, W. I. F. David, K. R. Ryan, M. O. Jones, P. P. Edwards, H. Chu and P. Chen, *Inorg. Chem.*, 2010, **49**, 4319–4323; (*c*) H. Wu, W. Zhou and T. Yildirim, *J. Am. Chem. Soc.*, 2008, **130**, 14834–14839; (*d*) X. D. Kang, Z. Z. Fang, L. Y. Kong, H. M. Cheng, X. D. Yao, G. Q. Lu and P. Wang, *Adv. Mater.*, 2008, **20**, 2756–2759.

11 (*a*) Z. T. Xiong, G. T. Wu, Y. S. Chua, J. J. Hu, T. He, W. L. Xu and P. Chen, *Energy Environ. Sci.*, 2008, **1**, 360–363; (*b*) K. Shimoda, Y. Zhang, T. Ichikawa, H. Miyaoka and Y. Kojima, *J. Mater. Chem.*, 2011, **21**, 2609–2615.

12 H. V. K. Diyabalanage, T. Nakagawa, R. P. Shrestha, T. A. Semelsberger, B. L. Davis, B. L. Scott, A. K. Burrell, W. I. F. David, K. R. Ryan, M. O. Jones and P. P. Edwards, *J. Am. Chem. Soc.*, 2010, **132**, 11836–11837.

13 H. V. K. Diyabalanage, R. P. Shrestha, T. A. Semelsberger, B. L. Scott, M. E. Bowden, B. L. Davis and A. K. Burrell, *Angew. Chem., Int. Ed.*, 2007, **46**, 8995–8997.

14 J. Spielmann, G. Jansen, H. Bandmann and S. Harder, *Angew. Chem., Int. Ed.*, 2008, **47**, 6290–6295.
15 Q. Zhang, C. Tang, C. Fang, F. Fang, D. Sun, L. Ouyang and M. Zhu, *J. Phys. Chem. C*, 2010, **114**, 1709–1714.
16 R. V. Genova, K. J. Fijalkowski, A. Budzianowski and W. Grochala, *J. Alloys Compd.*, 2010, **499**, 144–148.
17 K. J. Fijalkowski and W. Grochala, *J. Mater. Chem.*, 2009, **19**, 2043–2050.
18 K. J. Fijalkowski, R. V. Genova, Y. Filinchuk, A. Budzianowski, M. Derzsi, T. Jaron, P. J. Leszczynski and W. Grochala, *Dalton Trans.*, 2011, **40**, 4407–4413.
19 X. Kang, J. Luo, Q. Zhang and P. Wang, *Dalton Trans.*, 2011, **40**, 3799–3801.
20 H. Wu, W. Zhou, F. E. Pinkerton, M. S. Meyer, Q. Yao, S. Gadipelli, T. J. Udovic, T. Yildirim and J. J. Rush, *Chem. Commun.*, 2011, **47**, 4102–4104.
21 Y. S. Chua, W. Li, G. Wu, Z. Xiong and P. Chen, *Chem. Mater.*, 2012, **24**, 3574–3581.
22 X. Kang, L. Ma, Z. Fang, L. Gao, J. Luo, S. Wang and P. Wang, *Phys. Chem. Chem. Phys.*, 2009, **11**, 2507–2513.
23 (*a*) D. Ravnsbaek, Y. Filinchuk, Y. Cerenius, H. J. Jakobsen, F. Besenbacher, J. Skibsted and T. R. Jensen, *Angew. Chem., Int. Ed.*, 2009, **48**, 6659–6663; (*b*) R. Černý, K. Chul Kim, N. Penin, V. D'Anna, H. Hagemann and D. S. Sholl, *J. Phys. Chem. C*, 2010, **114**, 19127–19133.
24 S. Liu, Y. Zhang, L. Sun, J. Zhang, J. Zhao, F. Xu and F. Huang, *Int. J. Hydrogen Energy*, 2010, **35**, 4554–4561.
25 A. C. Stowe, W. J. Shaw, J. C. Linehan, B. Schmid and T. Autrey, *Phys. Chem. Chem. Phys.*, 2007, **9**, 1831–1836.
26 Z. T. Xiong, Y. S. Chua, G. T. Wu, W. L. Xu, P. Chen, W. Shaw, A. Karkamkar, J. Linehan, T. Smurthwaite and T. Autrey, *Chem. Commun.*, 2008, 5595–5597.
27 W. J. Shaw, M. Bowden, A. Karkamkar, C. J. Howard, D. J. Heldebrant, N. J. Hess, J. C. Linehan and T. Autrey, *Energy Environ. Sci.*, 2010, **3**, 796–804.
28 J. Yang, X. Wang, J. Mao, L. Chen, H. Pan, S. Li, H. Ge and C. Chen, *J. Alloys Compd.*, 2010, **494**, 58–61.
29 H. Zhang, Y. S. Loo, H. Geerlings, J. Lin and W. S. Chin, *Int. J. Hydrogen Energy*, 2010, **35**, 176–180.
30 C. Wu, G. Wu, Z. Xiong, X. Han, H. Chu, T. He and P. Chen, *Chem. Mater.*, 2009, **22**, 3–5.
31 T. Kobayashi, I. Z. Hlova, N. K. Singh, V. K. Pecharsky and M. Pruski, *Inorg. Chem.*, 2012, **51**, 4108–4115.
32 W. J. Shaw, M. Bowden, A. Karkamkar, C. J. Howard, D. J. Heldebrant, N. J. Hess, J. C. Linehan and T. Autrey, *Energy Environ. Sci.*, 2010, **3**, 796–804.
33 (*a*) P. J. Fazen, J. S. Beck, A. T. Lynch, E. E. Remsen and L. G. Sneddon, *Chem. Mater.*, 1990, **2**, 96–97; (*b*) P. J. Fazen, E. E. Remsen, J. S. Beck, P. J. Carroll, A. R. McGhie and L. G. Sneddon, *Chem. Mater.*, 1995, **7**, 1942–1956.
34 (*a*) P. Mauron, F. Buchter, O. Friedrichs, A. Remhof, M. Bielmann, C. N. Zwicky and A. Zuttel, *J. Phys. Chem. B*, 2007, **112**, 906–910; (*b*) P. Martelli, R. Caputo, A. Remhof, P. Mauron, A. Borgschulte and A. Züttel, *J. Phys. Chem. C*, 2010, **114**, 7173–7177; (*c*) A. Züttel, S. Rentsch, P. Fischer, P. Wenger, P. Sudan, P. Mauron and C. Emmenegger, *J. Alloys Compd.*, 2003, **356–357**, 515–520; (*d*) A. Züttel, P. Wenger, S. Rentsch, P. Sudan, P. Mauron and C. Emmenegger, *J. Power Sources*, 2003, **118**, 1–7.

